*Q. J. R. Meteorol. Soc.* (2002), **128**, pp. 1–999 doi: 10.1256/qj.yy.n

# An Updated Length Scale Formulation for Turbulent Mixing in Clear and Cloudy Boundary Layers

By G. Lenderink[1]* and A. A. M. Holtslag[2]

[1]*Atmospheric Research Department, Royal Netherlands Meteorological Institute, The Netherlands*
[2]*Meteorology and Air Quality section, Wageningen University, The Netherlands*

(Received 1 July 2003; revised 10 January 2004)

Summary

A new mixing length scale is presented for turbulence closure schemes with special emphasis on neutral to convective conditions in clear and cloudy boundary layers. The length scale is intended for a prognostic turbulent kinetic energy closure. It is argued that present-day length scale formulations may easily fail in one of following limits: schemes based on a local stability measure (e.g., the Richardson number) display unrealistic behavior and instabilities in the convective limit. This strongly limits the representation of mixing in cloudy boundary layers. On the other hand, it is shown that non-local parcel methods may misrepresent mixing near the surface. The new length scale formulation combines local and nonlocal stability in a new way; it uses vertical integrals over the stability (the Richardson number) in a simple "parcel" framework. The length scale matches with surface layer similarity for near-neutral conditions and displays a realistic convective limit. The use of the length scale formulation can be extended well to cloudy boundary layers. The scheme is numerically stable and computationally cheap. The behavior of the length scale is evaluated in a Single Column Model (SCM) and in a high resolution Limited Area Model (LAM). The SCM shows good behavior in three cases with and without boundary layer clouds. The prediction of the near surface wind and temperature in the LAM compares favourably with tower measurements at Cabauw (the Netherlands).

Keywords: Turbulence Closure TKE

## 1. Introduction

Higher order turbulence closures in weather prediction and climate model are receiving increasing attention (e.g., Therry and Lacarrere 1983; Bougeault and Lacarrère 1989; Bélair *et al.* 1999; Cuxart *et al.* 2000; Grenier and Bretherton 2001; Abdella and McFarlane 2001; Lenderink and Holtslag 2000). The simplest version (which is relatively cheap in computational demands) is a TKE-l scheme, which combines a prognostic equation of Turbulent Kinetic Energy (TKE or $E$) with a diagnostic length scale $l_{m,h}$ to compute the eddy diffusivity for momentum and heat.

Despite the more advanced physics introduced by the higher order TKE equation, it is still not well understood how to model the corresponding length scale, and proposals combine rather ad-hoc arguments (often based on matching) and/or simple physical concepts. For example, in the ECHAM4 scheme the length scale is chosen such that the TKE scheme matches with the Louis scheme near the surface. The main reasons for that ad-hoc matching procedure is that i) the Louis scheme yields sufficiently realistic behavior close to the surface (Beljaars and Holtslag 1991), and ii) the Louis scheme can be well adjusted (tuned) to the needs of operational models (e.g., Beljaars and Viterbo 1998). However, Lenderink *et al.* (2000) showed that the ECHAM4 TKE scheme displays large instabilities in an idealized case of Stratocumulus, caused by the interaction between the cloud physics and the length scale formulation, which is to a large extend based on the local Richardson number (see Section 2 for details). The strong dependency of turbulent mixing on local stability may amplify noise on a grid point level,

* Corresponding author: Royal Netherlands Meteorological Institute, De Bilt, 3730 AE, The Netherlands Country.

eventually leading to numerical instability. The generation of noise by turbulence schemes is a rather general problem in cloudy boundary layers (see e.g. Lenderink *et al.* 2004, in this issue).

Besides the numerical disadvantage of a strong dependency of the length scale on local stability, the physics behind this concept might also be questioned. In unstable conditions, the length scale at a certain height is constrained by the size of largest eddies; close to inversion, the length scale should therefore be limited by the presence of the inversion. In ECHAM4 the length scale only "feels" changes in local stability; there is no clear non-local control of the length scale.

A natural way to incorporate non-local stability into the length scale is proposed by Bougeault and Lacarrère (1989) (hereafter B&L). In this method, the length scale is computed from the distances which an upward and a downward adiabatic parcel can travel before being stopped at a level where it has lost all its kinetic energy by buoyancy effects. In this way, the stability of a whole layer is incorporated into the length scale. This method is physically appealing since it is based on the simple concept that the major part of transport is done by the largest eddies. The scheme has been tested extensively in convective boundary layers with good results. However, since mainly buoyancy enters the B&L length scale formulation, it will not react strongly to changes in the wind shear. With a usual TKE scheme this may easily give rise to conflicts with surface layer scaling for neutral to convective conditions (see Section 2).

Summarizing, the B&L length scale for unstable conditions is in a sense extremely non-local. It is mainly determined by the boundaries of the mixing domain. The scheme appears to have problems in reflecting a proper surface layer scaling for neutral to convective conditions. On the other extreme, the ECHAM4 length scale formulation is extremely local. This scheme has rather good surface layer characteristics, but also suffers from instability higher up in the atmosphere. The matter of local versus non-local impacts on the mixing coefficient has been put forward by Delage (1997) and has also been studied in a TKE scheme by Bélair *et al.* (1999): To what extend should local and non-local stability characteristics enter the $K$ (or length scale) formulation? In the following we will use the term local and non-local always in this sense. (In literature, non-local is frequently used to denote non-local transport other than local K-diffusion; see e.g., Deardorff (1972); Holtslag and Moeng (1991); Holtslag and Boville (1993). It should be carefully noted that, unless explicitly mentioned, we do not use the term non-local for non-local transport in this paper.)

In the current paper we will present a length scale formulation that may serve as an in-between; it uses local stability (the Richardson number) in a non-local framework. The application of the scheme is restricted to near-neutral conditions near the surface and convective conditions. For strongly stable (with $Ri > 0.2$) we rely on a separate length scale formulation (see Appendix B). We will illustrate the behavior in some idealized cases: a diurnal cycle of dry (convective) BL, a diurnal cycle of a Cumulus topped boundary layer, and a quasi-stationary case of a near-decoupled Stratocumulus cloud-topped boundary layer. In addition, we will show that the concept can be successfully applied to a regional atmospheric climate model (RACMO) and compare results to near surface measurements at the Cabauw tower (the Netherlands).

## 2. Turbulent mixing on basis of a TKE-l scheme

As a start we introduce a version of the TKE-l scheme which is widely used in literature. The TKE equation is given by (see e.g., Stull 1988):

$$\frac{\partial E}{\partial t} = \underbrace{-\overline{u'w'}\frac{\partial U}{\partial z} - \overline{v'w'}\frac{\partial V}{\partial z}}_{S} + \underbrace{\frac{g}{\theta_v}\overline{w'\theta'_v}}_{B} \underbrace{- \frac{\partial}{\partial z}(\overline{w'E} + \overline{w'p'}/\rho)}_{T} - \underbrace{\epsilon}_{D}, \tag{1}$$

The shear production S, the buoyancy production/consumption B, the transport T by turbulence and pressure forces, and the dissipation D (or $\epsilon$) are parameterized by

$$\begin{aligned} -\left[\overline{u'w'}\frac{\partial U}{\partial z} + \overline{v'w'}\frac{\partial V}{\partial z}\right] &= K_m\left[\left(\frac{\partial U}{\partial z}\right)^2 + \left(\frac{\partial V}{\partial z}\right)^2\right] \\ \frac{g}{\theta_v}\overline{w'\theta'_v} &= -K_h\frac{g}{\theta_v}\frac{\partial \theta_v}{\partial z} \equiv -K_h N^2 \\ -\frac{\partial}{\partial z}(\overline{w'E} + \overline{w'p'}/\rho) &= 2K_m\frac{\partial E}{\partial z} \\ \epsilon &= c_d\frac{E^{3/2}}{l_m}, \end{aligned} \tag{2}$$

with $c_d$ a constant, $l_{m,h}$ the mixing length for momentum/heat and $K_{m,h}$ the eddy diffusive for momentum/heat, defined by

$$K_{m,h} = l_{m,h}\sqrt{E}. \tag{3}$$

Note that we have absorbed all proportionality coefficients in $K$ into the length scale formulation. The factor 2 in the transport term is added to account for the effects of the pressure induced transport of $E$. Also note the definition of the Brunt-Vaisala frequency $N^2$ in Eq. (2).

The surface boundary condition for TKE is given by

$$E_{surf} = c_o u_*^2 + 0.2 w_*^2, \tag{4}$$

with $c_o = 3.75$. Here $u_*$ is the surface friction velocity, and $w_*$ is the convective velocity scale. In neutral conditions, and taking the limit to the surface, one arrives at a balance between shear production and dissipation:

$$\frac{u_*^4}{K_m} = c_d\frac{E^{3/2}}{l_m} \tag{5}$$

With $K_m = l_m\sqrt{E}$ and $E = E_{surf} = c_o u_*^2$ one obtains $c_d = c_o^{-2}$.

In ECHAM4 the length scale is given by

$$l_{m,h}(z) = \lambda(z) S_{m,h}(Ri)$$

with $\lambda(z)$ the Blackadar (1962) length scale and $S_{m,h}(Ri)$ a stability function derived from a matching with the Louis (1979) scheme at the surface; see Roeckner *et al.* (1996) for the definitions of $\lambda(z)$ and $S_{m,h}(Ri)$. Thus, the length scale is determined by the local Richardson number and the height above the surface. For unstable conditions $S_{m,h}$ is not bounded, which implies that the

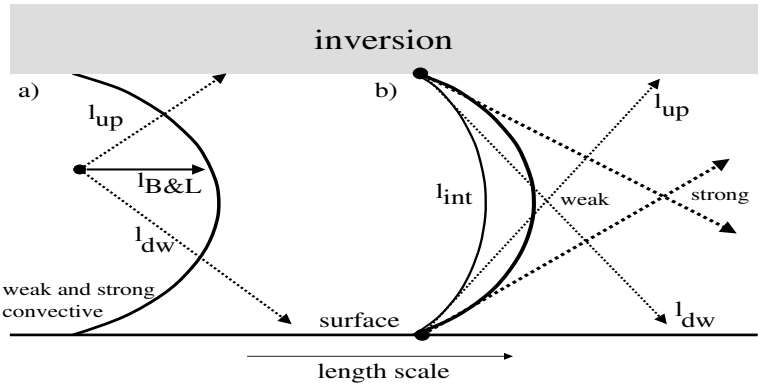


Figure 1. Illustation of a) the B&L length scale and b) the updated length scale in a convective case (see main text for details). In the B&L length scale formulation two parcels are released at *each* model level: $l_{up}$ and $l_{dw}$ denote the distances these parcel can travel. The parcels $l_{up}$ and $l_{dw}$ are combined to get a quadratic shape for the total mixing length (solid line). The updated length scale formulation uses *two* "parcels" only: one starts at the inversion, the other at the surface. Thick lines corresponds to a strongly convective, thin lines to a more neutral situation. Similar to the B&L proposal they are combined to obtain the final length scale $l_{int}$.

mixing length scale can take very large values. In particular, for cloud topped boundary layers this easily leads to numerical instability (for details see Lenderink *et al.* 2000).

In Bougeault and Lacarrère (1989) the length scale is computed from the distances which an upward and a downward adiabatic parcel can travel before being stopped at a level where it has lost all its kinetic energy by buoyancy effects. In the original proposal in Bougeault and Lacarrère (1989) the length scale (for heat and momentum) is composed from the minimum of the upward and the downward length scale, but in later implementations other averaging methods have also been used: e.g. in Cuxart *et al.* (2000) $\sqrt{l_{up}l_{dw}}$ is used. In unstable conditions the B&L length scale is mainly controlled by the distances to the surface and to the inversion (see Fig. 1a).

Using the TKE scheme described above, conflicts with surface layer similarity theory may arise if the upward and downward length scale proposed by Bougeault and Lacarrère (1989) are combined with the averaging operator given by Eq. 6 (or similar forms). To exploit this further, consider a boundary layer starting from neutral conditions and evolving into convective by increasing the surface heat flux (but retaining the same wind forcing). It can be shown based on surface layer similarity (see Appendix) that, in this framework, the length scale near the surface should become larger with increasing instability. However, near the surface the downward B&L length scale will not change since the downward parcel will not experience any deceleration due to buoyancy and will always hit the ground. With the used averaging operator there will be a distance close to the surface so that the length scale is fully determined by the downward length scale (as is trivial with the minimum operator originally proposed by B&L). So, in this framework and in this mathematical limit, the implementation of B&L in Eq.(6) leads to conflicts with surface similarity theory. In Meso-NH the surface layer behavior is improved by taking other averaging operators (Bougeault, personal communication).

## 3. The new length scale

The updated length scale formulation $l_{int}$ (computed from vertical integrals) represents mixing in the range from near-neutral to unstable conditions. It is computed from "averaging" over two length scales $l_{up}$ and $l_{dw}$ by:

$$\frac{1}{l_{int}} = \frac{1}{l_{up}} + \frac{1}{l_{dw}}. \tag{6}$$

These two length scale are defined as integrals over stability by:

$$\begin{aligned} l_{up} &= \int_{z_{bottom}}^{z} F(Ri)dz' \\ l_{dw} &= \int_{z}^{z_{top}} F(Ri)dz' \end{aligned} \tag{7}$$

where $F(Ri)$ is a function of the local Richardson number that will be defined below, and $z_{bottom}$ and $z_{top}$ are the lower and upper boundary of the mixing domain (also defined more precisely below).

First let us inspect how the length scale is designed to behave. We illustrate the behavior of the length scale in Fig. 1b in the (simplest) case of a convective boundary layer capped by a strong inversion. In that case $z_{top}$ is the inversion height $z_{inv}$, and $z_{bottom}$ is the surface. If, for the moment, we assume that $F$ is a constant $c$, than (for $z < z_{inv}$)

$$\begin{aligned} l_{up} &= cz \\ l_{dw} &= c(z_{inv} - z) \\ l_{int} &= c\frac{z}{z_{inv}}(z_{inv} - z) \end{aligned} \tag{8}$$

In this respect our method can be considered as a "poor man's" parcel method, obtaining rather similar results for convective situations to B&L, though at a much lower computational cost. Note that $l_{int}$ in this case is consistent with the results found for clear convective boundary layers (e.g., Holtslag and Moeng 1991).

To ensure that the length scale is influenced by local stability, we have to assume that $F$ depends on the Richardson number $Ri$. In Fig. 1b two situations are shown, one strongly convective case representative for a midday situation (thick lines), one only weakly convective case (thin lines) representative for the late afternoon. In these two situations, the behavior of $l_{up}, l_{dw}$ and $l_{int}$ is shown. So roughly, $F$ increases when the boundary layer becomes more unstable. In the following we will define $F$ in such a way that the resulting length scale obeys both the neutral limit and the convective limit.

We consider the mixing of momentum first, and propose the following form:

$$\begin{aligned} F_m(Ri) &= \\ &\alpha_n - \tfrac{2}{\pi}(\alpha_c - \alpha_n)(\alpha_r Ri), && Ri > 0 \\ &\alpha_n - \tfrac{2}{\pi}(\alpha_c - \alpha_n)\arctan(\alpha_r Ri). && Ri \leq 0. \end{aligned} \tag{9}$$

The function $F_m$ is plotted in Fig. 2. In this equation, the **n**eutral limit is determined by $\alpha_n$, and the convective limit determined by $\alpha_c$. The factor $\frac{2}{\pi}(\alpha_c - \alpha_n)\alpha_r$ determines the stability dependency near neutral. For stable conditions

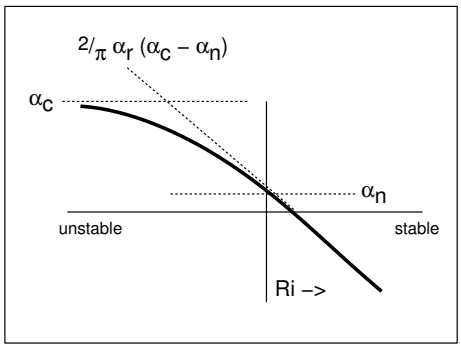


Figure 2. Functional dependency of F on the Richardson number $Ri$. The constants $\alpha_n$, $\alpha_c$ and $\frac{2}{\pi}(\alpha_c - \alpha_n)\alpha_r$ determine the neutral limit, the convective limit, and the stability dependency near neutral, respectively.

$F_m$ becomes negative for $Ri > Ri_{crit} \equiv \alpha_n/(\frac{2}{\pi}\alpha_r(\alpha_c - \alpha_n))$. Physically, Eq. (7) can be interpreted as a very simple "growth" rate equation for the length scale, with turbulence developing from the boundaries of the mixing domain and $F_m$ measuring the rate of growth dependent on local stability. Negative values for $Ri > Ri_{crit}$ imply a decaying turbulent length scale. Despite the fact that a precise physical interpretation is hard to give, the basic property of Eq. (7) seems physically sound; that is, mixing (the length scale) is determined by a mixture of local and nonlocal stability properties.

To determine the constants $\alpha_n$ and $\alpha_r$, we match to the linearized flux profiles relations in near neutral conditions. In Appendix A we derive that, close to the surface, the length scale should then obey

$$l_m = c_n \kappa z (1 - bRi) \tag{10}$$

Here $b \approx 4 - 5$ (see Appendix A).

We now choose $F_m$ so that $l_{int}$ matches with Eq. (10). By construction $l_{int} \approx l_{up}$ close to the surface. By matching Eq. (10) to Eq. (7) and filling in the definition of $F_m$:

$$\alpha_n z - \frac{2}{\pi}(\alpha_c - \alpha_n)\alpha_r \int_0^z Ri(z')dz' = c_n \kappa z - c_n \kappa z b Ri. \tag{11}$$

The first term on the left and right-hand side gives $\alpha_n = c_n\kappa$. The second term is linear in Ri at the right-hand side, but depends on an integral over the Ri on the left-hand side. Depending on how Ri depends on the height $z$ above the surface, a different matching is obtained. If we first assume Ri to be constant with height, we get

$$\alpha_r = \frac{\pi}{2}\frac{c_n\kappa}{\alpha_c - c_n\kappa}b \tag{12}$$

On the other hand, in particular for unstable conditions [see Eqs. (A.2,A.3) in Appendix A], we expect a linear variation of $Ri$ with height, so that

$$\alpha_r = \frac{\pi}{2}\frac{c_n\kappa}{\alpha_c - c_n\kappa}2b \tag{13}$$

These two values give a typical range for $\alpha_r$: differing a factor of 2 between the conservative estimate by Eq. (12) and the larger value by Eq. (13).

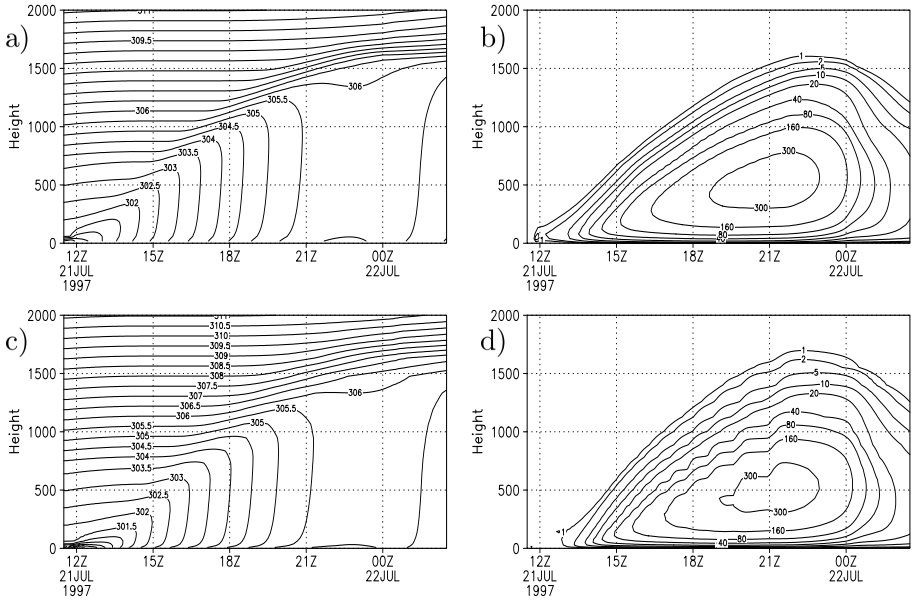


Figure 3. The diurnal cycle of a dry convective BL with shear. Time evolution of $\theta$ (K) (right-hand panels) and $K_h$ ($\mathrm{m^2 s^{-1}}$) (left-hand panels) at high vertical resolution (upper panels) and coarser vertical resolution (lower panels)

Despite the fact that Eq. (13) might seem more appropriate, we use the rather conservative estimate by Eq. (12), with a value of $b = 4$ as our reference value. Model experiments show that in particular for shallow boundary layers the downward length scale $l_{dw}$ has a considerable influence on the behavior of $l_{int}$ close to the surface, therefore violating the assumption $l_{int} \approx l_{up}$ on which the derivation is based. This results in a stronger stability dependency than expected from the matching argument. Some results obtained with Eq. (13) (with an adaptation in the downward length scale to force $l_{int} \approx l_{up}$ close to the surface) are also presented in Section 6. Finally, we choose $\alpha_c = 3c_n\kappa$. With this value the maximum of $K_m$ reaches approximately $0.1hw_*$ (with $h$ the dry boundary layer height) in a dry convective boundary layer.

The boundaries of the mixing domain are specified in following way. For $l_{up}$ we integrate $F_m$ from the surface upward. If $l_{up}$ becomes negative it is reset to zero, and the integration continues. At a certain height above, $l_{up}$ may become positive again if $F_m$ is positive. This is the case if $Ri < b^{-1} \equiv Ri_{crit}$ [0.25 with Eq. (12) and b = 4]. The procedure is continued until the top level of the model. The integration of $l_{dw}$ is done similarly, but starts at the top level of the model. In practice, this means that $l_{dw}$ starts to be nonzero at the level where $Ri = Ri_{crit}$. Note that this is rather commonly used value of $Ri_{crit}$ to identify the boundary layer top (see e.g., Vogelezang and Holtslag 1996). For heat we use the same value for $\alpha_n$ and $\alpha_r$. In the convective limit, we use $Pr \simeq 0.6$ (see e.g., Cuxart *et al.* 2000), which implies $\alpha_c = 5c_n\kappa$.

The integral length scale formulation does not apply in (strongly) stably stratified conditions, generally with $Ri > Ri_{crit}$ (as defined above). (Note that if a shallow stable layer exists within an unstable boundary layer, as is the case in

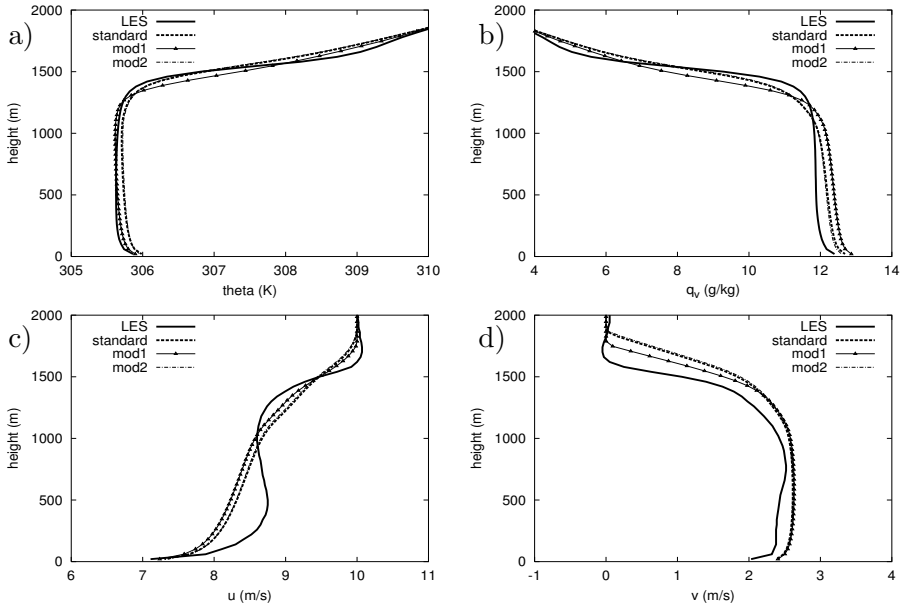


Figure 4. Comparison of potential temperature $\theta$, water vapor $q_v$, and horizontal winds at 21.30 UTC (15.30 LT) between the LES and different versions of the SCM (see main text for details).

section 5a, the integral length scale is nonzero in that stable layer.) Therefore we use for (strongly) stable conditions a generally accepted form based on local stability and TKE. This length scale and the way it is matched to the integral length scale is described in Appendix B. For the moment we remark that the stable length scale only plays a role in and above the inversion for convective conditions and near the surface for very stable conditions. In all other case, $l_{int}$ is mainly determining the turbulent length scale $l_{m,h}$.

## 4. Results for a clear boundary layer

To show the behavior of the TKE scheme with the updated length scale, a diurnal cycle over land is modelled. The case is derived from an intercomparison in GCSS (GEWEX Cloud System Study) Working Group 1, in which the time evolution of the diurnal cycle of shallow Cumulus clouds over land is investigated (Brown *et al.* 2002). This case, based on measurements at the ARM Southern Great Plains site (USA), is also used for a SCM intercomparison in Lenderink *et al.* (2004). Because, for the moment, we are not interested in clouds, we lowered the specific humidity of the initial profile by 4.7 g kg$^{-1}$, uniform in the vertical, except above 2400 m where this procedure leaded to negative specific humidity (in which case we reset to zero). This case has been run with the KNMI Large Eddy Simulation (LES) model as used in the ARM intercomparison paper by Brown *et al.* (2002). This procedure effectively prevented the occurrence of clouds in the LES model, but at the same time retaining the gradients in specific humidity in the area of interest (below the inversion). (In the next section we will investigate the original GCSS WG-1 ARM case.) The surface sensible and latent heat fluxes are prescribed, going through a diurnal cycle (max. at midday of 140 W m$^{-2}$ and

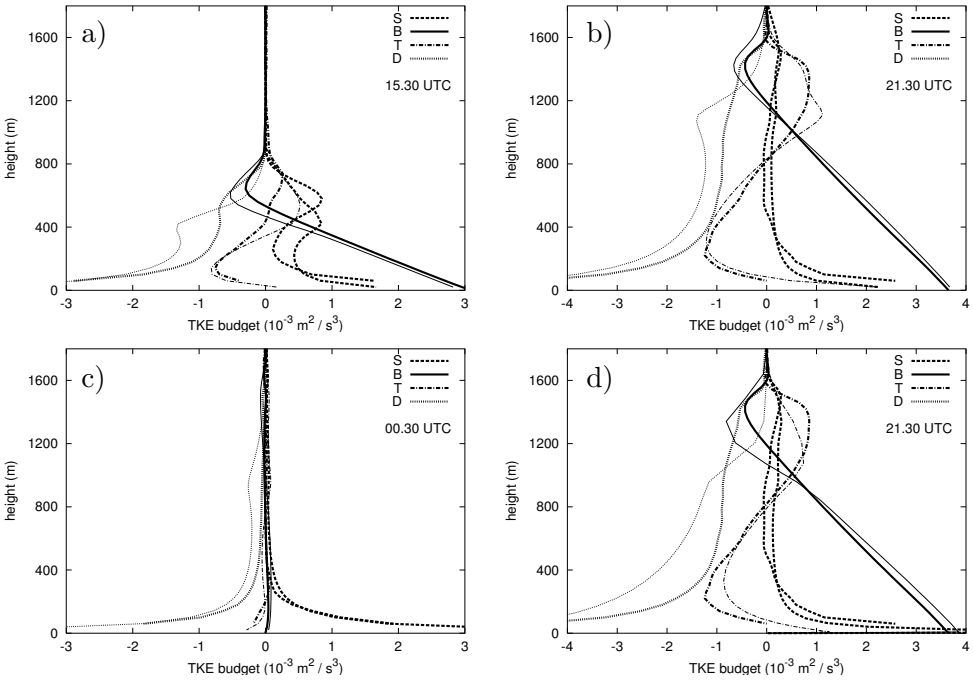


Figure 5. TKE budget with shear production (S), buoyancy (B), transport (T) and dissipation (D) at high resolution (a,b,c) and low resolution (d). Thick lines are LES results; thin lines the SCM results.

500 W m$^{-2}$, respectively). A geostrophic wind (u,v) of (10,0) m s$^{-1}$ is prescribed, together with a surface roughness of 0.035 m.

In Fig. 3a we show the time evolution of the potential temperature in the SCM model. Initialized from a stable profile at night, the evolution of the convective boundary is clearly seen, with a boundary layer height, starting near the surface a growing until 1000 meter at noon local time (18 UTC) and 1400 m at late afternoon (00 UTC). The LES results (not shown here) are very similar; the main difference is the slightly stable potential temperature profile in the upper part of the convective BL in the LES (counter gradient fluxes), whereas the SCM retains an slightly unstable profile until the base of the inversion layer. The inclusion of a nonlocal transport term (e.g., Deardorff 1972; Holtslag and Moeng 1991; Cuijpers and Holtslag 1998) could alleviate this fact. The eddy diffusivity for heat $K_h$ is shown in Fig. 3b. A smooth development of $K_h$ corresponding to the different stages of the boundary layer (stable to unstable to neutral and stable) is shown, thus demonstrating the good numerical stability characteristics of the scheme. At mid afternoon (21 UTC) $K_h$ has an almost quadratic profile with a maximum of 360 m$^2$s$^{-1}$. With a maximum value of $w_*$ of 1.9 m s$^{-1}$ this corresponds to about 0.12 h $w_*$. For momentum, $K_m$ has a very similar structure, but peaks at around 0.08 h $w_*$.

The profiles of temperature, water vapor, and the horizontal wind at mid afternoon (21.30 UTC) are shown in Fig. 4. In addition to the standard model tuning, we also performed a sensitivity run (*mod1*) with $c_h = 0.1$ in Eq. (B.1) which reduces the mixing in stable conditions. In a second sensitivity run (*mod2*)

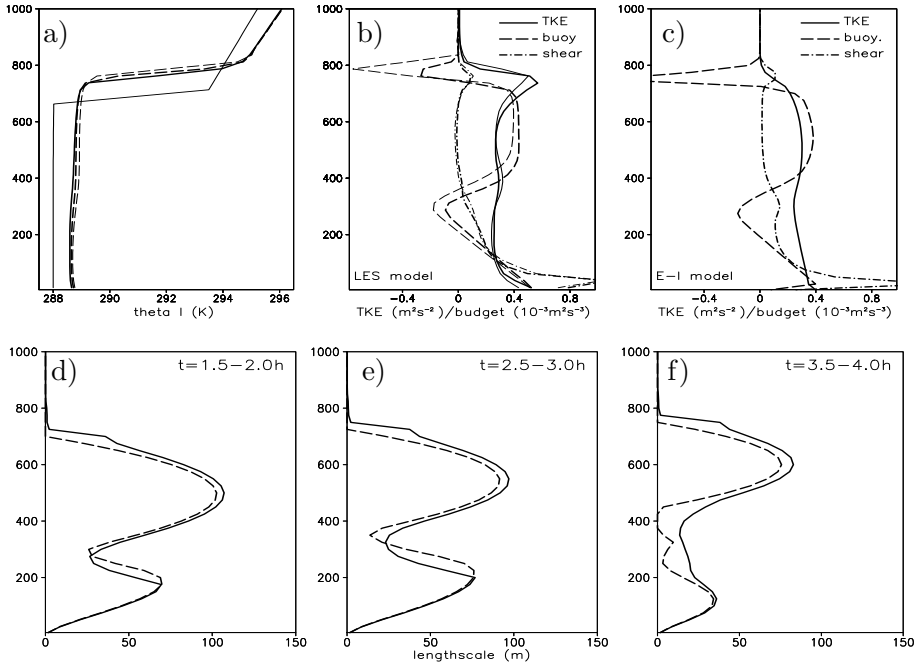


Figure 6. A Stratocumulus topped boundary layer. Average profiles during the third hour of the liquid water potential temperature (a) (solid line: SCM, two dashed lines: LES, and thin line: initial profile), TKE, and shear and buoyancy production for two LES models (b) and the SCM (c). The lower panels (d, e, f) show the length scales $l_{int}$ (dashed) and $l_h$ (final) (solid) during several stages of the simulation.

we used $\alpha_r$ given by Eq. (13). In generally, the results of this second sensitivity run (*mod2*) are almost indistinguishable from the standard run. The temperature and water vapor profiles are in rather good agreement with the LES results. It appears that the sensitivity run *mod1* has somewhat too small boundary layer height. In contrast, the boundary layer height in the standard run is about correct, but the moisture profile at the inversion for moisture is too diffuse.

The SCM results for $u$ do not support the well mixed (or even more than well mixed) profile in the middle of the convective boundary layer. The cause of this is that, in the absence of a nonlocal transport term, the SCM needs a positive gradient to sustain a downward momentum flux, so that future work on implementing nonlocal (non-downgradient) terms for momentum is recommended. Results for $v$ are better in agreement with the LES results. The small over-prediction of $v$ is mainly caused by a somewhat higher stress at the surface, causing a small over-prediction of the ageostrophic wind component.

Finally, in Fig. 5 we show at three different times shear production, dissipation, buoyancy and transport of $E$. The entrainment flux (negative buoyancy flux at the inversion) is somewhat large, in particular with shallow boundary layer (see plot at 15.30 UTC). The dissipation in the SCM results peaks in the upper part of the convective layer and is too small in the entrainment layer. Corresponding, the transport term has a peak at approximately the same height (or somewhat higher) as the peak in the dissipation. It is however not clear what is cause and effect; errors in dissipation and buoyancy flux could be caused by

the transport term. Shear production is reasonable with a small peak at the inversion (in particular during the first hours) and a large peak near the surface. Clearly, the TKE budget can be improved, in particular the parameterization of dissipation and transport seems to need some refinement. However, the SCM captures the main features of the TKE budget in the LES model. Results at the end of the afternoon in Fig. 5, representative for near neutral conditions, show that the TKE budget is almost fully determined by shear and dissipation, and that the transport of TKE is small.

These results have been obtained with high vertical resolution (50 m grid spacing) and small time step (60 seconds). To show that results are reasonably robust to the resolution and the time step, we included in Figs. 3c,d results on a coarser resolution (30 levels between the surface and 3000 m with approximately 120 m grid spacing at 1000 m) and with a 5 mn time step. The results are very close to the results on high resolution. The TKE budget shown in Fig. 5d shows the same basic features as obtained with the high resolution, although there are some significant differences in particular near the inversion where resolution becomes an important issue. But, as is shown in Fig. 3, the time evolution of the potential temperature field is very similar to the results on high resolution — indicating that the effective entrainment rate in both runs is similar. It should be noted that to take advantage of a TKE scheme, a comparatively high vertical resolution is needed (in particular in the cloudy case presented in the next section). The present scheme is not meant to perform optimally on coarse resolution, but is developed to remain stable at high vertical resolution. It is in this limit that many of the present operational schemes become numerically unstable (see Lenderink *et al.* 2004, in this issue).

## 5. Results for cloudy boundary layers

In this section we briefly illustrate the application of the length scale formulation in cloudy boundary layers. Before we can use the length scale formulation, the computation of the atmospheric stability has to be extended to moist conditions. To that purpose, the Brunt-Vaisala frequency $N^2$ is computed from the conserved variables total water $q_t$ and liquid water potential temperature (instead from $\theta_v$ directly):

$$N^2 = c_f \left( A_m \frac{\partial \theta_l}{\partial z} + B_m \frac{\partial q_t}{\partial z} \right) + (1 - c_f) \left( A_d \frac{\partial \theta_l}{\partial z} + B_d \frac{\partial q_t}{\partial z} \right)$$

with $A_d$, $A_m$, $B_d$ and $B_m$ as defined in Cuijpers and Duynkerke (1993) and $c_f$ is the layer cloud fraction. These constant are such that in dry conditions ($c_f = 0$) the buoyancy is mainly determined by $\theta_l$, whereas in moist conditions ($c_f = 1$) $q_t$ is equally important or even dominates stability. Thus, it is clear that local cloud fraction plays an important role. The cloud fraction is computed according to Cuijpers and Bechtold (1995)

$$c_f = \max\left(0, \min\left\{0.5 + 0.36 \arctan(1.55 \frac{q_t - q_{sat}}{\sigma_q}), 1\right\}\right)$$

with the $\sigma_q$ the square root the variance of $q_t$ given by

$$\sigma_q = \sigma_b + \sigma_{mf}. \tag{14}$$

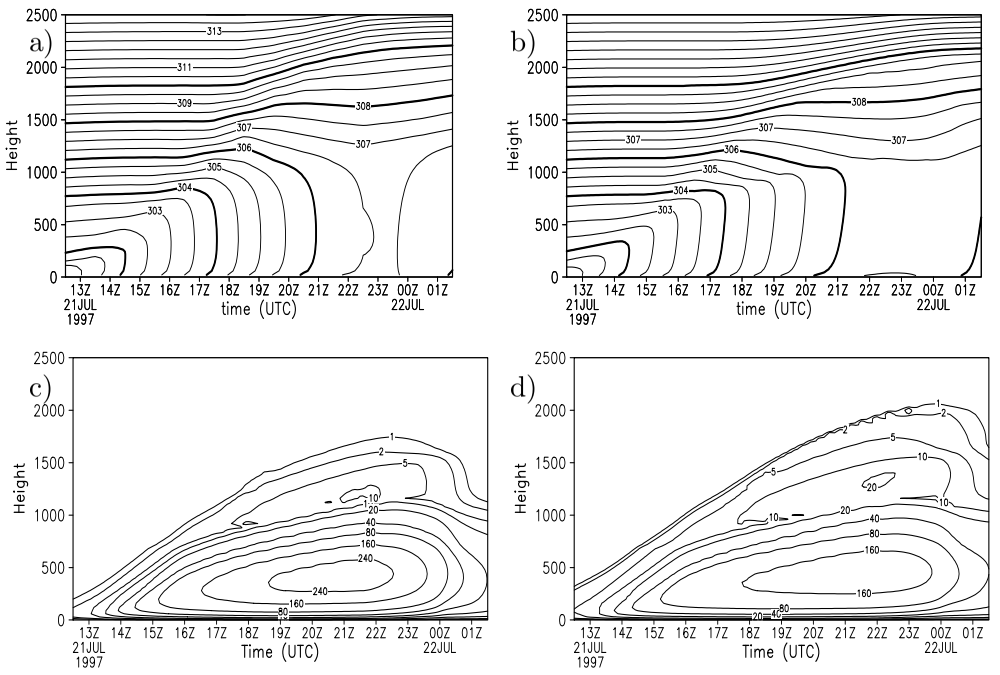


Figure 7. The diurnal cycle of a convective boundary layer with cumulus clouds. Time evolution of $\theta$ (K) in a) the LES and b) the SCM. Panel c) and d) show the eddy diffusivity $K_h$ ($\mathrm{m^2 s^{-1}}$) and $l_h$ (m) in the SCM model, respectively.

Here, $\sigma_b$ represents a small value due to turbulence or other processes, and $\sigma_{mf}$ is connected to the mass flux activity

$$\sigma_b = 0.02 q_{sat} \tag{15}$$

$$\sigma_{mf}^2 = -\frac{M \Delta q_t l_{cloud}}{w_*^{cu}} \frac{\partial q_t}{\partial z} \tag{16}$$

Here, $M$ is the mass flux, $\Delta q_t$ the difference in moisture between the updraft and the mean, $l_{cloud}$ the depth of the cloud layer, and $w_*^{cu}$ a convective velocity scale of the cloud layer (for details see Lenderink and Siebesma 2000):

$$(w_*^{cu})^3 = \int_{cloud} \frac{g}{\theta} M \Delta \Theta_v dz,$$

with $\Delta \Theta_v$ the difference in virtual potential temperature between updraft and environment. The mass flux scheme used is the Tiedtke (1989) scheme, but with the much higher entrainment and detrainment coefficients from Siebesma and Holtslag (1996).

### (*a*) *Stratocumulus topped boundary layer*

We consider a case with nocturnal stratocumulus clouds as defined in the EUCREM (EUropean Cloud-REsolving Modelling) model intercomparison project (Duynkerke *et al.* 1999). The case is based on observations made during the Atlantic Stratocumulus Transition Experiment (ASTEX) (Albrecht *et al.*

1995). The case description and results of LES models can be found in Duynkerke *et al.* (1999). In this case, the role of the cloud formulation is rather trivial since the cloud fraction is either close to one (in the cloud layer) or zero (elsewhere). The SCM is run with a 30 s time step and a resolution of 25 m.

The mean profile of the liquid water potential temperature $\theta_l$ during the third hour of the simulation is shown in Fig. 6. The SCM is able to resolve the typical structure of $\theta_l$ in the LES models. Also the cloud liquid water content and total water content $q_t$ are rather close to the LES results [not shown here, but close to Fig. 3 in Lenderink and Holtslag (2000)]. The profiles of TKE and the buoyancy and shear production terms are in Figs. 6 b, c. The buoyancy production in the SCM is practically identical to the LES results in the cloud and subcloud layer. In the entrainment zone the minimum of the buoyancy flux is more pronounced in the SCM, though it is noted that also the two LES models are also rather different in the inversion. The fact that the buoyancy fluxes in the (upper part) of the cloud in LES and SCM are very similar shows that the effective entrainment flux in the LES and in the SCM are almost the same. In the LES, shear production peaks at the surface, but there is also a small peak close to the inversion. The SCM model is able to capture these two maxima, but adds a smaller (not supported by LES) peak near cloud base. The mean value of TKE in the SCM is close to the LES results. However, the SCM model fails to reproduce the maximum in the LES results close to the inversion. In the LES this maximum is related to the variance of the horizontal winds. In the SCM a maximum near the inversion cannot co-exist with upward transport of TKE into the inversion since this transport is modelled with downgradient diffusion [see Lenderink and Holtslag (2000) for more on this issue].

During the integration the boundary layer depth increases and the cloud layer tends to decouple from the subcloud layer. During this process a small, stable layer develops at cloud base. In Figs. 6 d, e, f we show at three different times the integral length scale $l_{int}$ for heat and the total length scale $l_h$ (see Appendix B for the matching of the stable length scale and $l_{int}$) during the decoupling process. Both $l_{int}$ and $l_h$ reflect decoupling by producing a minimum in the subcloud layer. As the decoupling phase progresses the mixing lengths in the subcloud stable layer decrease, thereby promoting further decoupling. The new length scale continuously adapts to the changing stability profile. Therefore, the new length scale formulation allows a continuous transition between a coupled and decoupled stratocumulus layer. (Note that this would be different with a traditional parcel method, like Bougeault and Lacarrère (1989), since a parcel either penetrates or stops at the subcloud layer. In terms of the length scale decoupling would therefore be a discontinuous process.)

### (*b*) *Diurnal cycle of cumulus convection*

The final SCM case is the original ARM case (with the inclusion of clouds) as discussed in Section 4. The case is described in Brown *et al.* (2002) and results of an intercomparison study of SCMs derived from (semi-) operation models, including results obtained with the present integral length scale formulation, are presented in Lenderink *et al.* (2004).

The time evolution of the potential temperature in the SCM and LES is shown in Fig. 7. The growth of a convective boundary layer is clearly visible. A cloud layer starts to develop during noon local time (18 UTC) with a corresponding conditionally unstable layer to 2000 m. The SCM captures both

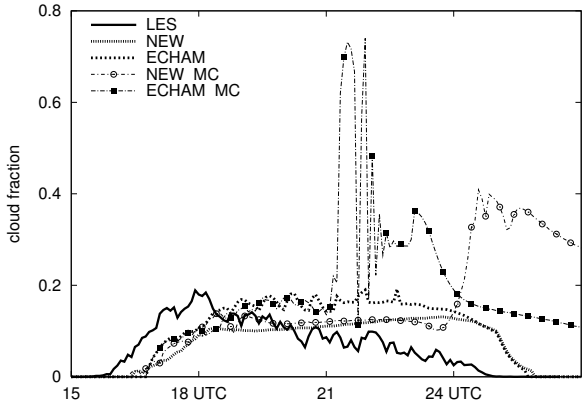


Figure 8. Timeseries of maximum cloud fraction in four SCM simulations.

the temperature structure of cloud and subcloud layer rather well. In Figs. 7 c,d we show the eddy diffusivity $K_h$ and the length scale $l_h$ for heat. Both are large in the subcloud layer, with a maximum at 40 % of the dry boundary layer height. In the cloud layer both $K_h$ and $l_h$ reduce to smaller, but still significant values.

The TKE scheme, and in particular the length scale formulation, behaves continuously in time and space. This contrast to the results of several operational models presented in Lenderink *et al.* (2004) for the same case. To illustrate the stability behavior of our length scale, we compare to results obtained with the ECHAM4 length scale formulation (with otherwise the same model formulation). The time evolution of maximum cloud cover is shown in Fig. 8. Compared to the LES results, the cloud amount is about correct in the SCM, though the SCM fails to reproduce a maximum in cloud cover early noon with a gradual decrease in the afternoon. The results obtained with the ECHAM4 formulation contain slightly more noise, but this may be not very significant.

Next, we repeat the experiment with a different closure for the mass flux scheme. Instead of the closure based on the velocity scale of the subcloud layer (Grant 2001; Neggers *et al.* 2003), we switched to the subcloud moisture convergence closure as is presently used in the ECHAM4 physics package (Roeckner *et al.* 1996). With this closure, subcloud turbulence and mass flux activity start to interact more strongly. The results dramatically change. With the ECHAM4 formulation a strong instability occurs at 15 local time (21 UTC). This instability is visible in profiles of potential temperature and atmospheric humidity as a (close to) stepfunction. For example, at 2000 m the atmospheric water vapor increases from 8 to 12 g kg$^{-2}$ in 15 minutes time. This behavior is not caused by an inversion passing this level, but it is due to a short period of extremely strong mixing which drastically changes the profiles in the whole cloud layer. In the new formulation there is tendency toward higher cloud fractions at the end of the simulation, and a small oscillation superimposed, but there is no sign of instability in the thermodynamic profiles. The atmospheric temperature and humidity profiles evolve smoothly in time. The feedback loop giving rise to this the increase in cloud cover with time is described extensively in Lenderink *et al.* (2004).

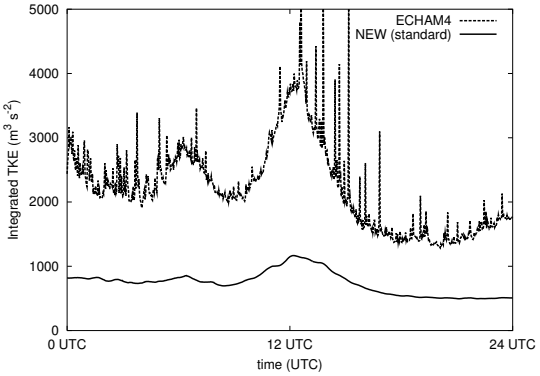


Figure 9. Time evolution of the vertically integrated TKE (domain averaged) for a typical day (22 Feb).

The results underline the fact that it is the interaction between turbulence scheme and other schemes (e.g. cloud scheme, condensation, mass flux scheme and radiation) that might lead to instability. The updated length scale formulation is better able to cope with small disturbances introduced by other parts of the physics and has a stronger damping effect on these disturbances.

## 6. Comparison with Cabauw tower data

An intercomparison between model predictions and measurements at the Cabauw tower is performed for February 2001. To that purpose, we have implemented the turbulence scheme described above in the KNMI limited area regional atmospheric model (RACMO). This model uses the ECHAM4 physics package (Roeckner *et al.* 1996) embedded in HIRLAM dynamics (Christensen *et al.* 1996). We ran the model in a forecast cycle (without data assimilation) starting each day at 12 UTC from the ECMWF analysis field. Each 36-h forecast used ECMWF analysis fields as lateral boundaries (updated each 6 h). We use output of the model from +12 h to +36 h. The forecast cycle starts 12 UTC on 31st January 2001. The vertical resolution is 40 levels (near the surface at

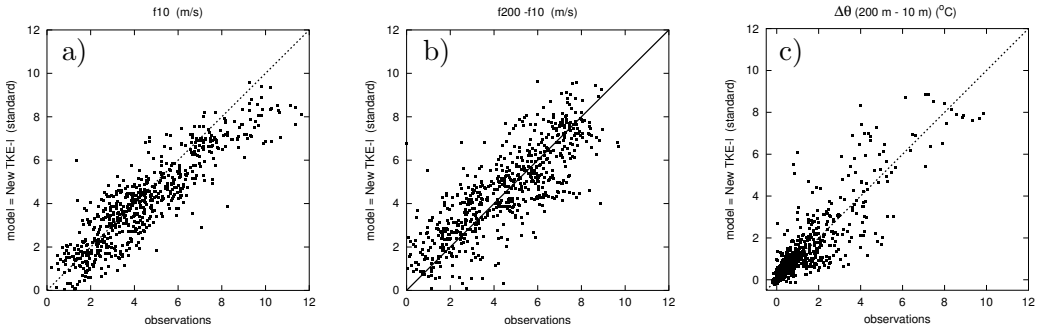


Figure 10. Scatter plot (model against observations) of a) the 10m wind speed, b) the wind speed difference and c) potential temperature difference between 200m and 10m as obtained with the new scheme.

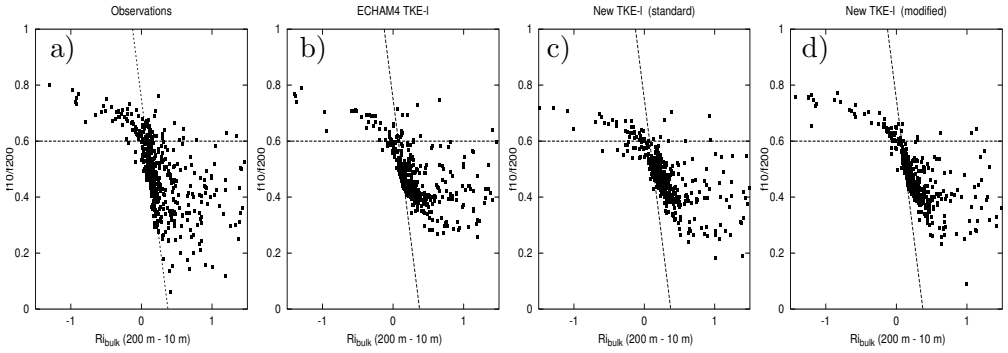


Figure 11. Ratio between 10 m wind and 200 m wind as function of the bulk Richardson number.

approx. 10, 35, 125, 190, 270 m) and the horizontal resolution is 18 km. The model domain is about 1000x1000 km$^2$, centered around the Cabauw tower. For reference, we also performed a similar model integration using the ECHAM4 length scale formulation.

The Cabauw tower is a 200 m meteorological tower situated at Lopik ($51^o58'$ N, $4^o56'$ E) in the Netherlands. Continuous measurements of temperature, humidity and winds are made at different heights. We averaged both model data and measurements over a 1-h period in order to filter out the high frequency variations, in particular in the measurements. The terrain around Cabauw has a surface roughness of about 0.06-0.30 m, depending on the direction (van Ulden and Wieringa 1996). The model uses a constant roughness of 0.07 m at the grid point nearest to Cabauw. The first days of February 2001 are characterized mostly by weakly stable and neutral conditions, whereas in the second half of the month also more convective situations occur.

Results of the domain averaged, vertically integrated TKE show a high level of intermittency in the simulation with the ECHAM4 turbulence scheme as shown in Fig. 9 for a typical day (22 Feb 2001). This is numerical noise, rather than that it is due to the intermittency of turbulence since the TKE scheme should represent the statistical average of turbulence. The average value of TKE over a large domain should be even more continuous in time. The new scheme does not suffer from this instability, and shows a reasonable (numerically stable) evolution in time.

In Fig. 10 we show model results (obtained with the new scheme) against observations of the 10 m wind (f10) and wind speed difference between 200 m and 10 m (f200 - f10). On overage results are reasonably good, but there appears to be a systematic underestimation of the wind speed at high wind velocities. We computed for each day the RMS error and the bias (based on hourly averages), and averaged these over the month. Monthly mean biases in f10 and in (f200 - f10) are -0.4 m s$^{-1}$and -0.3 m s$^{-1}$, respectively. RMS errors in 10m wind and the wind speed difference are 1.1 m s$^{-1}$and 1.3 m s$^{-1}$, respectively. Model results obtained with the ECHAM4 length scale formulation are very similar (and are therefore not shown) with monthly mean biases and RMS errors within 0.05 m s$^{-1}$. The potential temperature difference between 200 m at 10 m is plotted

in Fig.10c. On average, the model shows a reasonable skill to predict the near surface temperature gradient.

As a more demanding measure of the model behavior of winds, we study the ratio between f10 and f200 (hereafter, $R_{wind}$) as a function of the bulk Richardson number between 200 and 10 m. In neutral conditions and with a roughness length of 0.05 - 0.30 m, this ratio is 0.63-0.53 when a logarithmic wind profile is assumed. In Fig. 11 we show results for the Cabauw measurements (a), for the model integrations with the ECHAM4 turbulence scheme (b), the new turbulence scheme (c), and a modified version (to be discussed below) of the new scheme (d) (As a guide to the eye, we included in each plot the same line drawn through the bulk of the tower measurements.). Compared to the measurements, the model integrations show a reasonable stability dependency in the range from neutral to weakly stable conditions. The variations in $R_{wind}$ are to some extent underpredicted in all model versions. Also for more stable conditions they under predict the variability in $R_{wind}$.

Finally, we consider the dimensionless wind gradient $\phi_m$ as a function of $z/L$, with $L$ the Monin-Obhukov length and the normalized wind gradient

$$\phi_m = \frac{\kappa z}{u_*} \left| \frac{\partial \bar{U}}{\partial z} \right| . \tag{17}$$

Since we do not have reliable measurements of the surface stress and surface heat flux for the period considered, we could not do this analysis for the measurements. For the model results, the gradients are computed between the three pairs of levels closest to the surface: so between 10 m and 35 m, between 35 and 70 m, and between 70 and 125 m. Results are shown in Fig. 12 for the ECHAM4 turbulence scheme (a) and the new scheme (b) and the modified version of the new scheme (c). As a reference we also plotted the commonly used flux profile relation $1 + 5z/L$ for stable conditions. On average, the data obtained with the ECHAM4 turbulence scheme are rather close to this line for weak stability, and bent off for higher stability consistent with earlier findings, as e.g. discussed in Beljaars and Holtslag (1991). The latter is related to tuning of the scheme with more mixing in stable condition than can be motivated based on flux profile measurements, which appears to be necessary for the skill of operational models (see e.g. Holtslag *et al.* 2003).

The results of the new scheme (standard version) show significantly more scatter with a wide range of $\phi_m$ values between $1 + 5z/L$ and $1 + 2z/L$. Analysis showed that this range is caused by the influence of the downward length scale $l_{dw}$ on the integral turbulent length scale [see Eq. (6)]. To illustrate this we pragmatically set $l_{dw}$ on a minimum value near the surface:

$$l_{dw} = \max(\, l_{dw}, 75\, e^{-z/500}\,) \tag{18}$$

This artificially removes the influence of $l_{dw}$ near the surface, and forces $l_{int}$ to be close to $l_{up}$. This procedure does not have any significant influence on deeper convective boundary layers, and results for the SCM cases presented are practically identical. However, removing the influence of $l_{dw}$ invalidates the motivation for taking the conservative estimate of $\alpha_r$. Consequently we utilize Eq. (13) from now on. Results of $R_{wind}$ and $\phi_m$ obtained with this modified version are shown in Fig. 11d and in Fig. 12c, respectively. (Plots for the temperature and wind are very similar to the reference version and are therefore

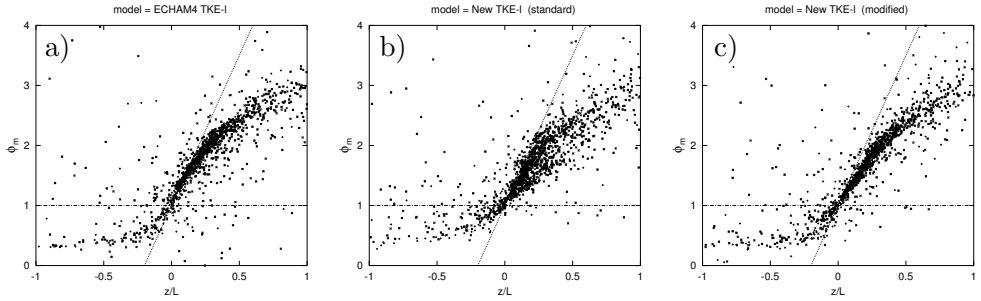


Figure 12. Flux profile relation $\phi_m$ as a function of $z/L$ computed directly from model output.

not shown.) Fig. 12c shows that the dimensionless wind gradient is now in much closer agreement with the flux profile relations, and is in every sense comparable to the ECHAM4 scheme. It is also important to note that, although the matching was only obtained by a linearization near neutral conditions, the resulting length scale seems valid for a much larger stability range.

Is should be noted that the flux profile relations were obtained under stationary conditions, often with strongly filtered measurements. Whether the scatter in the model data is a realistic feature or not is therefore hard to say since we did not perform any filtering on the model data (to the cases for which surface layer similarity is applicable).

## 7. Summary and conclusions

We have presented an updated length scale formulation intended for a TKE-l turbulence closure. The scheme displays realistic behavior near the surface, is numerically stable and computationally cheap. Its main application is to neutral (and weakly stable) and convective clear and cloudy boundary layers. For strongly stable (generally with $Ri > 0.2$) the length scale formulation is overridden by a seperate length scale formulation (see Appendix B), and we realize that future improvements may be needed for the (very) stable side (e.g. Holtslag *et al.* 2003).

In contrast to most length scale formulations, stability enters the length scale formulation in a non-local, vertically integrated sense. This significantly improves the numerical stability characteristics of the scheme. For convective conditions, the length scale formulation mimics the behavior of the Bougeault and Lacarrère (1989) length scale (hereafter B&L length scale), though at a much lower computation cost. It is argued that the main weakness of the B&L length scale is the marginal stability dependency of the length scale formulation in the range from neutral to convective situations (see Fig. 1a of this paper). This complicates matching to surface layer similarity (see Appendix A). The stability dependency in our scheme enables a matching to surface layer similarity in a rather broad range around neutral conditions. On the downside, with the separation into the updated (integral) length scale formulation and the seperate formulation for stable conditions a rather arbitrary matching between these to formulations is needed (see Appendix B). However, the latter problem could be circumvented – at the cost of an increase in computational demands – by

introducing the B&L parcels in our the framework and a suggestion is made in Appendix B.

The single column model results obtained with the new scheme show realistic behavior in three cases: i) a diurnal cycle of dry convective boundary layer, ii) a diurnal cycle of convective boundary layer with cumulus clouds, and iii) a simulation of near-decoupled Stratocumulus clouds. In addition, near surface results of a limited area model using the new scheme compare favourably with measurement at the Cabauw tower. Near the surface the scheme behaves comparable to the ECHAM4 scheme, but with significantly lower levels of noise higher up in the atmosphere. This appears to be a significant advantage when simulating boundary clouds and cloud related fields (see also Lenderink *et al.* 2000, 2004). The present scheme is implemented in the latest versions of the reference HIRLAM system (Unden *et al.* 2002).

## Acknowledgements

Discussions with Fred Bosveld, Pier Siebesma and Colin Jones, and the constructive comments of two anonymous reviewers, are kindly acknowledged. The first author acknowledges financial support from the EU funded project EUROCS (EVK2-CT-1999-00051).

## Appendix A

### *Surface Layer Matching*

Using surface layer similarity we can express the diffusivity coefficients as (see e.g., Holtslag 1998)

$$K_m = \frac{(\kappa z)^2}{\phi_m^2}\left|\frac{\partial \bar{U}}{\partial z}\right| \tag{A.1}$$

where $\phi_m$ is the dimensionless wind gradient. Using the commonly accepted flux profile relations by Dyer (1974)

$$\begin{aligned} \phi_m = \phi_h &= 1 + 5\tfrac{z}{L} && \text{stable} \\ \phi_m &= (1 - 16\tfrac{z}{L})^{-1/4} && \text{unstable} \\ \phi_h &= (1 - 16\tfrac{z}{L})^{-1/2} \end{aligned} \tag{A.2}$$

and using

$$Ri = \frac{z}{L}\frac{\phi_h}{\phi_m^2} \tag{A.3}$$

to express z / L in terms of $Ri$ we arrive at

$$K_m \approx (\kappa z)^2(1 - 2bRi)\left|\frac{\partial \bar{U}}{\partial z}\right| + O(Ri^2). \tag{A.4}$$

Here we linearized near neutral conditions. Strictly $b$ is 5 for stable and 4 for unstable conditions, but, for means of simplicity and considering all the other uncertainties in the length scale formulation, we just took one value for $b$ for stable and unstable conditions.

Assuming stationarity of the TKE equation, neglecting the transport of TKE, and using the definitions of S, B, D in Eq. (1), one can rewrite the TKE equation as

$$\frac{B}{D} = \frac{B/S}{1 + B/S + T/S} = \frac{-Ri_f}{1 - Ri_f} \tag{A.5}$$

where $Ri_f \equiv -B/S$. If we rewrite $Ri_f = Pr^{-1}Ri$ we have

$$\frac{-Ri}{1 - Pr^{-1}Ri} = \frac{PrB}{D} = \frac{l_m^2 N^2}{c_d E} \tag{A.6}$$

This gives

$$E = \frac{l_m^2 N^2}{c_d}\left(\frac{1 - Pr^{-1}Ri}{Ri}\right) = \frac{l_m^2}{c_d}(1 - Pr^{-1}Ri)\left|\frac{\partial \bar{U}}{\partial z}\right|^2 \tag{A.7}$$

For the eddy diffusivity this means

$$K_m = l_m\sqrt{E} = \frac{l_m^2}{{c_d}^{1/2}}\sqrt{1 - Pr^{-1}Ri}\left|\frac{\partial \bar{U}}{\partial z}\right|. \tag{A.8}$$

This form is similar to Eq. (A.4) based on the linearized flux profile relations. If we match Eq. (A.8) with Eq. (A.4), and use that $b' >> 0.25$ and $Pr \simeq 1$ in near neutral cases, we finally achieve

$$l_m \simeq {c_d}^{1/4}\kappa z(1 - bRi) + O(Ri^2) \tag{A.9}$$

Here we define a constant $c_n \equiv c_d^{1/4}$, so that for neutral conditions $K_m = ku_* z$ is obtained with $l_m = c_n \kappa z$. By approximating $\sqrt{1 - Pr^{-1}Ri} \simeq 1$, the TKE balance reduces to $E = D$. Thus, for our matching procedure it is sufficiently accurate to assume a balance between shear production and dissipation.

By multiplying Eq. A.7 by $E$, one obtains

$$E^2(z) = c_o^2(1 - Pr^{-1}Ri)K_m^2\left|\frac{\partial \bar{U}}{\partial z}\right| = c_o^2 u_*^4(z)(1 - Pr^{-1}Ri). \tag{A.10}$$

with $u_*(z)$ the momentum stress at height $z$. Thus, the equilibrium value of $E$ is consistent with the surface boundary condition imposed by Eq. (4).

## Appendix B

### *Length scale for stable conditions*

For stably stratified conditions a separate length scale formulation needs to be employed on basis of local stability and turbulent kinetic energy. Then the general accepted form is:

$$l_s = c_{m,h}\frac{\sqrt{E}}{N} \tag{B.1}$$

where $c_{m,h}$ is a constant not necessarily the same for heat and momentum. We took $c_h = 0.2$ as a standard value. We also performed sensitivity runs with half this value: $c_h = 0.1$. For momentum we took $c_m = c_h Pr = c_h(1 + 2Ri)$ (but limited at $3c_h$). The dependency of the Prandtl number $Pr$ on $Ri$ is added to represent the mixing of momentum by wave activity. Data presented by Kim and Mahrt

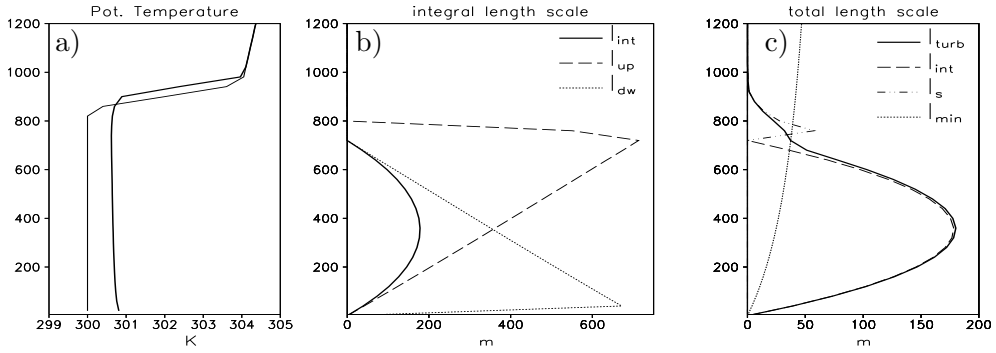


Figure B.1. SCM profiles in a convective BL for a) theta, b) $l_{int}$, $l_{up}$ and $l_{dw}$, and c) the resulting final length scale $l_{turb}$, and its compontents $l_{int}$, $l_{min}$ and $l_s$.

(1992) and Schumann and Gerz (1995) suggest a dependency of about 2-4 $Ri$. This dependency increases mixing under very stable conditions, which appears to be important for the forecast skill of AGCMs (Beljaars and Viterbo 1998; Delage 1997). On the other hand, other measurements (Nieuwstadt 1984) and flux profile relations (Dyer 1974) imply an almost constant Prandtl number. Note that Nieuwstadt (1984) selected only for stronger wind speeds above 5 m $s^{-1}$.

The turbulent length scale $l_{m,h}$ combines the integral length scale $l_{int}$ and the stable length scale $l_s$ in the following way. The interpolation is a slightly modified (see below) version of

$$\frac{1}{l_{m,h}} = \frac{1}{\max(l_{int}, l_{min})} + \frac{1}{l_s} \tag{B.2}$$

with $l_{min}$ defined below and $l_s^{-1} = 0$ for unstable conditions. Basically this interpolation limits $l_{m,h}$ to $(l_{min}^{-1} + l_s^{-1})^{-1}$ in stable conditions, and to $l_{int}$ for unstable conditions. The use of $l_{min}$ is necessary because for very stable conditions $l_{int}$ is zero, which would unrealistically limit $l_{m,h}$ if $l_{m,h} = (l_{int}^{-1} + l_s^{-1})^{-1}$ is used. The length scale $l_{min}$ is chosen such that close to the surface it does not limit $l_{int}$ which represent mixing also for weakly stable conditions. Therefore we use the following expression (similar to Blackadar 1962)

$$\frac{1}{l_{min}} = \frac{1}{l_\infty} + \frac{1}{0.5 c_n \kappa z}. \tag{B.3}$$

with $l_\infty = 75$ m. Note that close to the surface, the length scale is limited to half the neutral length scale $c_n \kappa z$.

For the actual model implementation, we took a more continuous interpolation by:

$$\frac{1}{l_{m,h}^p} = \frac{1}{[(l_{int}^q + l_{min}^q)^{1/q}]^p} + \frac{1}{[l_s]^p} \tag{B.4}$$

The first term on right hand side limits on $\max(l_{int}, l_{min}) 2^{1/q}$, so that for the limit $q \to \infty$ a max statement is retrieved. We used $q = 2$, which is in fact already close to a max statement if $l_{int}$ is twice as large as $l_{min}$. For $p$ we used 2 (instead of 1 used above), which reduces the influence of $l_s$ close to the surface. In particular, for weakly stable stratification, $l_s$ already had a significant impact on $l_{m,h}$, which intervenes with $l_{int}$ which has been designed to handle this situation.

Results of a dry convective boundary layer shown in Fig. B.1 illustrate how the interpolation works. The simulation has no wind and moisture, and the surface heat flux amounts 60 W $m^{-2}$. The profile of potential temperature $\theta$, initially and after 2.5 h of simulation, is shown in Fig.B.1a. Shown is a typical growth of the boundary layer height, a well mixed layer (with slightly unstable profile in order to promote upward heat flux). Figs. B.1b,c show the length scales for heat: $l_{int}$ composed from $l_{up}$ and $l_{dw}$ in Fig.B.1b, and the interpolation in Fig. B.1c. Shown are an almost linear increase of $l_{up}$ from the surface to base of the entrainment layer (here defined by the level at which the atmosphere becomes stable; that is, where the buoyancy flux becomes negative). Similarly, $l_{dw}$ increases linearly from the base of the entrainment layer to the surface. The resulting $l_{int}$ is approximately quadratic. The stable length scale formulation $l_s$ (Fig. B.1c) limits the length scale in the inversion, but also has a singularity where the profile is only slightly stable. This is also a reason for limiting on the length scale on $l_{min}$. Fig. B.1c shows that the interpolation by Eq. (B.4) supports a continuous interpolation between i) $l_{int}$ in the convective boundary layer, and ii) $l_s$ is the (upper part of the) inversion layer with iii) a rather smooth transition in-between.

Despite the fact that the interpolation of $l_s$ and $l_{int}$ using $l_{min}$ is to some extent artificial, in particular near the inversion, the results are not very dependent on $l_{min}$. For example, running the dry convective case of section 4 with $l_\infty = 300$ m (effectively doubling $l_{min}$ at 1000 m) increases the entrainment flux (minimum of the buoyancy flux compared to the surface flux) at 21 UTC from 20 % in the standard run to 24 %. Using $l_\infty = 35$ m (reducing $l_{min}$ to 60 % at 1000 m) the entrainment flux reduces to 17 %.

Finally, the B&L parcels could be introduced in the framework given by Eq. (7) by letting $l_{bottom}$ and $l_{top}$ be determined by the upward and downward B&L parcels. In this case, the stability function $F$ would have to be redefined at the stable limit, but with $F \rightarrow$ constant for the stable limit, automatically (B.1) is retrieved. In this procedure there is no need for a seperate stable length scale formulation; however, this would re-introduce the computational demands of B&L since $l_{bottom}$ and $l_{top}$ would now have to be computed for each grid level.

## References


Abdella, K. and McFarlane, N. 2001 Modelling boundary-layer clouds with a statistical cloud scheme and a second-order turbulence closure. *Boundary-Layer Meteorology*, **98**, 387–410

Albrecht, B. A., Bretherton, C. S., Johnson, D., Schubert, W. H. and Frisch, A. S. 1995 The Atlantic Stratocumulus Transition Experiment - ASTEX. *Bull. of the Amer. Met. Soc.*, **76**, 889–904

Bélair, S., Mailhot, J., Strapp, J. W. and MacPherson, J. I. 1999 An examination of local versus nonlocal aspects of a TKE-based Boundary Layer scheme in clear convective conditions. *J. Appl. Meteor.*, **38**, 1499–1518

Beljaars, A. C. M. and Holtslag, A. A. M. 1991 Flux parameterization over land surfaces for atmospheric models.. *J. Appl. Meteor.*, **30**, 327–341

Beljaars, A. C. M. and Viterbo, P. 1998 'The Role of the Boundary Layer in a Numerical Weather Prediction Model'. Pp. 287–304 in *Clear and Cloudy Boundary Layers*, Eds. A. A. M. Holtslag and P. G. Duynkerke, Royal Netherlands Academy of Arts and Sciences

Blackadar, A. K. 1962 The vertical distribution of wind and turbulent exchange in a neutral atmosphere. *J. Geophys. Res.*, **67**, 3095–3102

| | | |
|---|---|---|
| Bougeault, P. and Lacarrère, P. | 1989 | Parameterization of Orography-Induced Turbulence in a Mesobeta-Scale model. *Mon. Wea. Rev*, **117**, 1872–1890 |
| Brown, A. R., Cederwall, R. T., Chlond, A., Duynkerke, P. G., Golaz, J.-C., Khairoutdinov, J. M., Lewellen, D. C., Lock, A. P., Macvean, M. K., Moeng, C.-H., Neggers, R. A. J., Siebesma, A. P. and Stevens, B. | 2002 | Large-eddy simulation of the diurnal cycle of shallow cumulus convection over land. *Quart. J. Roy. Met. Soc.*, **128(B)**, 1075–1094 |
| Christensen, J. H., Christensen, O. B., Lopez, P., van Meijgaard, E. and Botzet, M. | 1996 | 'The HIRHAM4 regional atmospheric climate model'. Tech. Rep. 96-4 DMI |
| Cuijpers, J. W. M. and Bechtold, P. | 1995 | A Simple Parameterization of Cloud Related Variables for Use in Boundary Layer Models. *J. Atmos. Sci.*, **52**, 2486–2490 |
| Cuijpers, J. W. M. and Duynkerke, P. G. | 1993 | Large-eddy simulation of trade-wind cumulus clouds. *J. Atmos. Sci.*, **50**, 3894–3908 |
| Cuijpers, J. W. M. and Holtslag, A. A. M. | 1998 | Impact of skewness and nonlocal effects on scalar and buoyancy fluxes in convective boundary layers. *J. Atmos. Sci.*, **55**, 151–162 |
| Cuxart, J., Bougeault, P. and Redelsperger, J.-L. | 2000 | A turbulence scheme allowing for mesoscale and Large-Eddy Simulations. *Quart. J. Roy. Met. Soc.*, **126**, 1–30 |
| Deardorff, J. W. | 1972 | Theoretical expression for the counter-gradient vertical heat flux. *J. Geophys. Res.*, **77**, 5900–5904 |
| Delage, Y. | 1997 | Parameterising sub-grid scale vertical transport in atmospheric models under statically stable conditions. *Boundary-Layer Meteorology*, **82**, 23–48 |
| Duynkerke, P. G., Jonker, P. J., Chlond, A., van Zanten, M. C., Cuxart, J., Clark, P., Sanchez, E., Martin, G., Lenderink, G. and Teixeira, J. | 1999 | Intercomparison of three- and one-dimensional model simulations and aircraft observations of stratocumulus. *Boundary-Layer Meteorology*, **92**, 453–487 |
| Dyer, A. J. | 1974 | A review of flux-profile relationships. *Boundary-Layer Meteorology*, **7**, 363–372 |
| Grant, A. L. M. | 2001 | Cloud-base fluxes in the cumulus-capped boundary layer. *Quart. J. Roy. Met. Soc.*, **127**, 407–422 |
| Grenier, H. and Bretherton, C. S. | 2001 | A Moist PBL Parameterization for Large-Scale Models and Its Application to Subtropical Cloud-Topped Marine Boundary Layers. *Mon. Wea. Rev*, **129**, 357–377 |
| Holtslag, A. A. M. | 1998 | 'Modelling of Atmospheric Boundary Layers.'. Pp. 85–110 in *Clear and Cloudy Boundary Layers*, Eds. A. A. M. Holtslag and P. G. Duynkerke, Royal Netherlands Academy of Arts and Sciences |
| Holtslag, A. A. M., Beare, R. J. and Cuxart, J. | 2003 | GABLS workshop on Stable Boundary Layers.. *GEWEX Newsletter*, **13 (4)**, 11–13 |
| Holtslag, A. A. M. and Boville, B. A. | 1993 | Local versus nonlocal boundary-layer diffusion in a global climate model.. *J. Climate*, **6**, 1825–1842 |
| Holtslag, A. A. M. and Moeng, C.-H. | 1991 | Eddy diffusivity and countergradient transport in the convective atmospheric boundary layer. *J. Atmos. Sci.*, **48**, 1690–1698 |
| Kim, J. and Mahrt, L. | 1992 | Simple formulation of turbulent mixing in the stable free atmosphere and nocturnal boundary layer. *Tellus*, **44A**, 381–394 |
| Lenderink, G. and Holtslag, A. A. M. | 2000 | Evaluation of the kinetic energy approach for modelling turbulent fluxes in Stratocumulus. *Mon. Wea. Rev*, **128**, 244–258 |
| Lenderink, G., van Meijgaard, E. and Holtslag, A. A. M. | 2000 | Evaluation of the ECHAM4 cloud-turbulence scheme for Stratocumulus. *Meteor. Zeitschrift*, **9**, 41–47 |

| | | |
|---|---|---|
| Lenderink, G. and Siebesma, A. P. | 2000 | 'Combining the Massflux Approach with a statistical cloud schemes'. Pp. 66–69 in Proceedings of 14th Symposium on Boundary Layers and Turbulence, Aspen, USA. Americal Meteorological Society |
| Lenderink, G., Siebesma, A. P. and Co-authors | 2004 | The diurnal cycle of shallow Cumulus clouds over land: A single column model intercomparison study. QJRMS (this issue) |
| Louis, J. F. | 1979 | A parametric model of vertical fluxes in the atmosphere. *Boundary-Layer Meteorology*, **17**, 187–202 |
| Neggers, R. A. J., Siebesma, A. P., Lenderink, G. and Holtslag, A. A. M. | 2003 | An evaluation of mass flux closures for diurnal cycles of shallow Cumulus. Accepted by Mon. Wea. Rev. |
| Nieuwstadt, F. T. M. | 1984 | The turbulent structure of the stable, nocturnal boundary layer. *J. Atmos. Sci.*, **41**, 2202–2216 |
| Roeckner, E., Bengtsson, L., Christoph, M., Claussen, M., Dumenil, L., Esch, M., Giorgetta, M., Schlese, U. and Schulzweida, U. | 1996 | 'The Atmospheric general circulation model ECHAM-4: Model description and simulation of present-day climate'. Tech. Rep. 218 Max-Planck-Institut fur Meteorologie |
| Schumann, U. and Gerz, T. | 1995 | Turbulent mixing in stably stratified shear flows. *J. Appl. Meteor.*, **34**, 33–48 |
| Siebesma, A. P. and Holtslag, A. A. M. | 1996 | Model Impacts of Entrainment and Detrainment Rates in Shallow Cumulus Convection. *J. Atmos. Sci.*, **53**, 2354–2364 |
| Stull, R. B. | 1988 | *An introduction to boundary layer meteorology*. Kluwer Academic Publishers, London & High Wycombe |
| Therry, G. and Lacarrere, P. | 1983 | Improving the eddy kinetic energy model for planetery boundary layer description. *Boundary-Layer Meteorology*, **25**, 63–68 |
| Tiedtke, M. | 1989 | A comprehensive mass flux scheme for cumulus parameterization in large-scale models. *Mon. Wea. Rev*, **177**, 1779–1800 |
| van Ulden, A. P. and Wieringa, J. | 1996 | Atmospheric boundary layer research at Cabauw.. *Boundary-Layer Meteorology*, **78**, 39–69 |
| Unden, P., Rontu, L. and 24 Co-authors | 2002 | 'HIRLAM-5 scientific documentation.'. Tech. rep. SMHI (S-601 76, Norrköping, Sweden) |
| Vogelezang, D. H. P. and Holtslag, A. A. M. | 1996 | Evaluation and model impacts of alternative boundary-layer height formulations.. *Boundary-Layer Meteorology*, **81**, 245–269 |